

Article

Boundary Conditions for Transient and Robust Performance of a Reduced-Order Model-Based State Feedback Controller with PI Observer

Nebiyeleul Daniel Amare , Doe Hun Kim , Sun Jick Yang  and Young Ik Son *

Department of Electrical Engineering, Myongji University, Yongin 17058, Korea; nebiyeleul1@gmail.com (N.D.A.); doehun94@naver.com (D.H.K.); sunny8841@naver.com (S.J.Y.)

* Correspondence: sonyi@mju.ac.kr; Tel.: +82-31-330-6358

Abstract: One common technique employed in control system design to minimize system model complexity is model order reduction. However, controllers designed by using a reduced-order model have the potential to cause the closed-loop system to become unstable when applied to the original full-order system. Additionally, system performance improvement techniques such as disturbance observers produce unpredictable outcomes when augmented with reduced-order model-based controllers. In particular, the closed-loop system stability is compromised when a large value of observer gain is employed. In this paper, a boundary condition for the controller and observer design parameters in which the closed-loop system stability is maintained is proposed for a reduced-order proportional-integral observer compensated reduced-order model-based controller. The boundary condition was obtained by performing the stability analysis of the closed-loop system using the root locus method and the Routh-Hurwitz criterion. Both the observer and the state feedback controller were designed using a reduced-order system model based on the singular perturbation theory. The result of the theoretical analysis is validated through computer simulations using a DC (direct current) motor position control problem.



Citation: Amare, N.D.; Kim, D.H.; Yang, S.J.; Son, Y.I. Boundary Conditions for Transient and Robust Performance. *Energies* **2021**, *14*, 2881. <https://doi.org/10.3390/en14102881>

Academic Editor: Luigi Fortuna

Received: 3 April 2021
Accepted: 7 May 2021
Published: 17 May 2021

Publisher's Note: MDPI stays neutral with regard to jurisdictional claims in published maps and institutional affiliations.



Copyright: © 2021 by the authors. Licensee MDPI, Basel, Switzerland. This article is an open access article distributed under the terms and conditions of the Creative Commons Attribution (CC BY) license (<https://creativecommons.org/licenses/by/4.0/>).

Keywords: proportional-integral observer; reduced-order model-based controller; stability analysis; Routh-Hurwitz criterion; dc motor; robust control

1. Introduction

Among the various factors determining the performance of a control system, model identification and accuracy in the design stage play a crucial role [1]. However, modeling real world systems is not always a convenient task due to the computational complexity that arises with the presence of certain dynamic characteristics. In such cases, model order reduction is applied through a numerical computation to transform the original system model into a more practical form that only captures the dominant characteristics and ignores dynamic behaviors that either contribute less or make the computation complex [2,3]. Such an order reduction enables fast and efficient parametric analysis of large-scale computational models [4–7]. Regardless of the computational complexity, ignoring dynamic characteristics that define a system's input output behavior exposes the model to a relative degree uncertainty causing the system performance to deteriorate under various circumstances. In other words, the neglected states in the reduction process give rise to an unmodeled dynamics with a known bound [8]. For this reason, the study of stability and performance improvement of reduced-order model-based controllers (ROMBC) is a worthy research topic. Moreover, the topic is timely as it can be applied for the system modeling and controller design of distributed systems found in innovative fields such as microfluidics [9].

1.1. Literature Review

On account of its ability to compensate for the undesirable effects caused by various classes of structured and unstructured uncertainties, disturbance observer-based control

(DOBC) technique has been widely used to restore nominal control system performance and numerous control studies have been presented on the topic [10–18]. To mention a few, in [14] a predesigned cascade scheme controller which was used to regulate the output voltage of a DC/DC boost converter was augmented with a reduced-order PIO to maintain the desired voltage regulation performance under various uncertainties. The modified control scheme successfully maintained nominal performance under the presence of plant uncertainties, such as load fluctuation, parametric uncertainties, unmodeled dynamics and input voltage variations. Similarly, [17], was able to improve the robustness of a predesigned cascade control scheme of a single axis magnetic levitation system by nesting a PIO in both the inner and outer-loop of the control system. Specifically, including an observer in both loops allowed the control system to regain nominal performance in the presence of system parameter uncertainties and external disturbances that existed in both loops.

The closed-loop stability of a DOBC has also been the topic of various researchers. In particular, Ref. [11] presents a sufficient condition for the closed-loop system stability of DOBC under the condition that the Q-filter has a sufficiently small time constant. The paper makes the argument that for the closed-loop stability, the uncertain plant should be of minimum phase, and for a given predesigned controller that can stabilize the nominal plant, robust stabilization can be achieved by an appropriate choice of low-pass filter without altering the controller.

Although there have been numerous studies performed on the performance improvement and stability analysis of DOBC subjected to system parameter uncertainty and external disturbance, there has only been few studies performed on the stability analysis of DOBC subjected to relative degree uncertainty caused by model order reduction (DOBC combined with ROMBC). One of these studies is presented in [19]. The paper studies robust stability of a DOBC when the relative degree of the plant is not the same as that of the nominal model. Contrary to expectations, it was pointed out in [19] that using a high-gain observer to compensate for the relative degree uncertainty caused by the model order reduction gives rise to closed-loop system instability. Specifically, Ref. [19] states that the closed-loop system becomes unstable with sufficiently fast Q-filter when the relative degree of the plant is unknown. Implying that the performance improvement effort of the observer risks destabilizing the closed-loop system.

The revelation made in [19] paves the way for further studies to be performed on the closed-loop system stability analysis of a DOBC system under the influence of relative degree uncertainty caused by model order reduction. Although the paper points out that using a high-gain observer for a DOBC with unknown relative degree of the plant risks making the closed-loop system unstable, it does not answer the question: How fast can the observer employed for restoring nominal performance to an ROMBC be before it risks destabilizing the closed-loop system? In other words, a specific boundary of the observer design parameter that will improve system robustness against relative degree uncertainty without risking closed-loop instability was not identified. Thus, this paper focuses on answering this particular question. This paper identifies the boundary of the observer design parameter in which the system robustness is improved without compromising closed-loop system stability.

1.2. Proposed Analysis

This paper presents the stability analysis of an ROMBC combined with a reduced-order PIO (ROPIO) to obtain the boundary of the design parameters of the observer and controller in which system performance is improved without compromising closed-loop system stability. The model order reduction undertaken in this paper is based on the singular perturbation approach [2,4]. A stability boundary condition based on the closed-loop system pole is established by applying the ROMBC to the original full-order system. Following the stability analysis, an ROPIO is designed separately to compensate for the effects of the relative degree uncertainty caused by the order reduction. Subsequently, the stability analysis of the ROPIO compensated ROMBC is performed to establish boundary

conditions based on the observer gain by using the Routh-Hurwitz stability criterion. The boundary conditions from the theoretical analysis reveals that the value of the observer gain must decrease as the feedback controller closed-loop pole increases. This implies that there exists a break from the separation principle for a reduced-order model-based observer and state feedback controller. It can be also said that an ROPIO designed using a reduced model is not capable of compensating for the relative degree uncertainty resulting from the order reduction.

The performances of both the ROMBC and the ROPIO compensated ROMBC are tested via a numerical example based on a DC motor position control problem through various computer simulations. The performance is examined by focusing on the transient state performance and disturbance rejection ability. From the mathematical analysis and the simulations carried out, the limitations of designing a controller and an observer using a reduced-order model is pointed out. Finally, a relatively desirable performance region based on the closed-loop pole and observer gain value is identified.

The contributions made by this paper can be summarized as follows:

1. Introducing a trade-off that exists between transient state performance and disturbance rejection ability in an observer compensated ROMBC through a mathematical analysis and a simulation based validation.
2. Presenting analysis that supports the break from the separation principle that exists for reduced-order model-based state feedback controller and observer.
3. Presenting a stability boundary condition for the closed-loop system based on the ROMBC closed-loop pole and ROPIO gain.
4. Proposing a relatively desirable performance region based on the values of closed-loop pole and observer gain for ROPIO compensated ROMBC.

The rest of the paper is organized as follows: Section 2 introduces the system model and presents the design of a reduced-order model-based state feedback controller. The stability analysis of the ROMBC is also presented in this section supported by a computer simulation to test the performance of the controller. Section 3 deals with the ROPIO designed for the purpose of restoring the nominal performance to the control system against the relative degree uncertainty. In Section 3.1 the ROPIO is designed and applied to the ROMBC. In this section, the drawbacks of applying a high-gain ROPIO on an ROMBC are shown via a computer simulation. Next, in Section 3.2 a stability analysis is performed on the ROPIO compensated ROMBC to shed a light on cause of the drawbacks observed in the simulation. Section 4 elaborates the theoretical analysis performed thus far by applying it to the position control problem of a DC motor. Through a series of simulations the section presents further discussions on the stability and disturbance rejection performance of the class of controllers under study. The paper is concluded in Section 5.

2. Reduced-Order Model-Based State Feedback Control

Consider the single-input linear time-invariant systems represented by

$$\begin{cases} \dot{x}_1 = x_2 \\ \dot{x}_2 = x_3 \\ \vdots \\ \dot{x}_{n-1} = x_n \\ \dot{x}_n = -a_1x_1 - a_2x_2 - a_3x_3 - \cdots - a_{n-1}x_{n-1} - a_nx_n + bu, \end{cases} \quad (1)$$

where x_i ($1 \leq i \leq n, n \geq 2$) is the system state, u is the control input, a_i ($1 \leq i \leq n$) and b are the system parameters.

When the parameter $a_n > 0$ has large magnitude, the dynamic characteristic of x_n behaves significantly faster than the rest of the states. Based on the singular perturba-

tion theory [2,4], the original model (1) is simply reduced to the following quasi-steady state model

$$\begin{cases} \dot{x}_1 = x_2 \\ \dot{x}_2 = x_3 \\ \vdots \\ \dot{x}_{m-1} = x_m \\ \dot{x}_m = \frac{1}{a_n}(-a_1x_1 - a_2x_2 - a_3x_3 - \dots - a_mx_m + b(u + d_r)), \end{cases} \tag{2}$$

where $m := n - 1$ ($m \geq 1$) and d_r represents an uncertainty resulted from the system order reduction.

Comparing the Laplace transforms of (1) and (2), the unstructured uncertainty (d_r) is obtained as

$$D_r(s) = -\frac{s}{b(s + a_n)}(-a_1X_1 - a_2X_2 - \dots - a_mX_m + bU(s)). \tag{3}$$

This paper investigates whether the mal-effects of d_r could be relieved by using a high-gain disturbance observer designed based on the reduced model (2).

Due to its simplicity, the reduced model is often considered to design a stabilizing control law. In order to have all the closed-loop poles at a certain location $s = -\alpha; \alpha > 0$, a state feedback control

$$u = -Kx_{[1,m]}; \quad x_{[1,m]} = [x_1 \quad x_2 \quad \dots \quad x_m]^T \tag{4}$$

is applied with $K = [k_1 \quad k_2 \quad \dots \quad k_m]$. Since the closed-loop system (2)–(4) yields the characteristic equation

$$s^m + \left(\frac{a_m + bk_m}{a_n}\right)s^{m-1} + \dots + \left(\frac{a_2 + bk_2}{a_n}\right)s + \frac{a_1 + bk_1}{a_n} = 0, \tag{5}$$

the feedback gains are set to

$$k_i = \frac{1}{b} \left(a_n \binom{m}{m-i+1} \alpha^{m-i+1} - a_i \right), \quad 1 \leq i \leq m, \tag{6}$$

where $\binom{m}{r} = \frac{m!}{r!(m-r)!}$.

Applying the ROMBC (4)–(6) to the original system (1) yields

$$\begin{cases} \dot{x}_1 = x_2 \\ \dot{x}_2 = x_3 \\ \vdots \\ \dot{x}_{n-1} = x_n \\ \dot{x}_n = -a_n\alpha^m x_1 - a_n \binom{m}{m-1} \alpha^{m-1} x_2 \dots - a_n \binom{m}{2} \alpha^2 x_{m-1} - a_n \binom{m}{1} \alpha x_m - a_n x_n, \end{cases} \tag{7}$$

where $m = n - 1$. The characteristic equation of the closed-loop system (7) is described by

$$s^n + a_n(s + \alpha)^m = 0. \tag{8}$$

In order to establish a relation between α and a_n , as well as to study the stability of (7), (8) is rearranged into a form more suitable for the root locus analysis as

$$1 + \frac{a_n(s + \alpha)^m}{s^n} = 0. \tag{9}$$

Out of n root trajectories starting from the origin, $m(= n - 1)$ move towards $-\alpha$ (multiple) and one towards $-\infty$. The departure angles are obtained as $(2k + 1)\pi/n$, where k is an integer number. Thus, when the system order $n \geq 3$, some of the root trajectories will move towards the right-half plane and turn to the left-half plane as a_n increases. Figure 1 shows the root locus of (9) when $n = 3$ and $\alpha = 1000$ for an example.

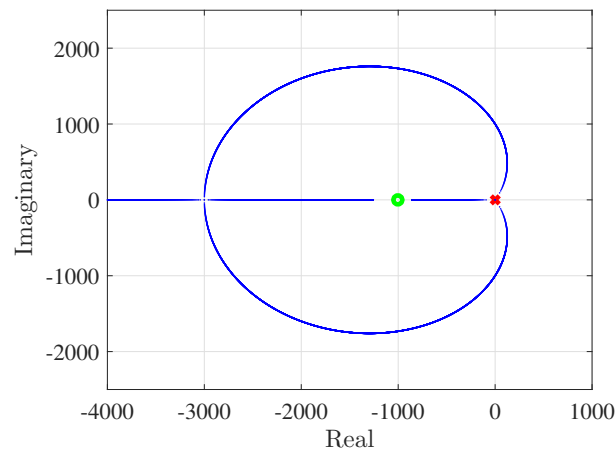


Figure 1. Root locus of (9) when $n = 3$ and $\alpha = 1000$.

To find the boundary condition for α that maintains the stability of (7), the Routh-Hurwitz criterion is applied to (8). Based on the analysis, a necessary condition is given by

$$a_n \binom{m}{1} \alpha - \binom{m}{2} \alpha^2 > 0. \quad (10)$$

According to (10), α must satisfy the condition below.

$$0 < \alpha < \frac{2a_n}{m-1}. \quad (11)$$

This means that the design parameter α in (6) is limited by the system parameter a_n .

Based on the above analysis, the performance of (4) has been tested on a DC motor position control problem as shown in Figure 2. The details of the computer simulations are discussed in Section 4.2. The figure shows the performance of (4) using three different values of α in $\{1000, 2000, 3000\}$, selected according to the stable range (11). In order to test the disturbance rejection ability, the system was subjected to a step disturbance at $t = 0.07$ s.

In Figure 2, the controller with a higher value of α is less susceptible to the external disturbance. On the other hand, the large value of α increases the overshoot at the transient state. This is the outcome of the relative degree uncertainty (3) resulted from the model reduction.

In such cases, a disturbance observer might be employed to recover the system performance owing to its ability to restore control performance against system uncertainties and disturbances [10,12]. In the next section a reduced-order proportional-integral observer (ROPIO) is designed using the reduced model (2) to deal with the unstructured disturbance.

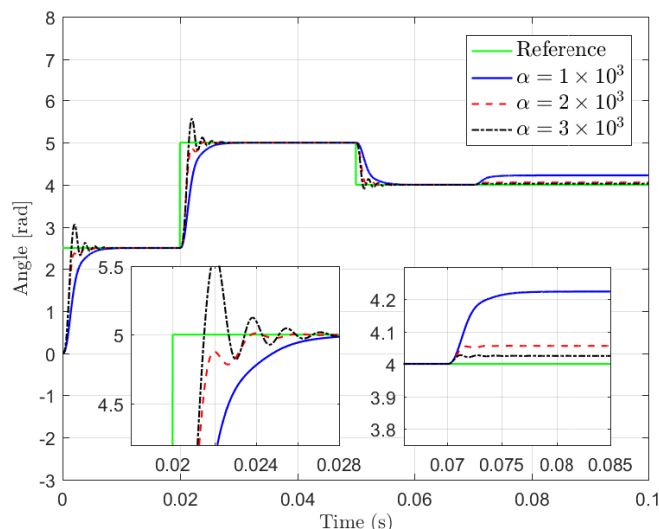


Figure 2. Transient and disturbance rejection performance of ROMBC (4).

3. Stability Conditions for an ROPIO Compensated ROMBC

3.1. Design of an ROPIO Compensated ROMBC

The system model (2) is subjected to an unstructured uncertainty (d_r) resulted from the system order reduction. In addition, it might also experience external disturbances and parameter uncertainties. To compensate for these effects, an ROPIO is designed separately from (4). By assuming a constant equivalent disturbance [10], the reduced-order system can be realized as

$$\begin{cases} \dot{x}_1 = x_2 \\ \dot{x}_2 = x_3 \\ \vdots \\ \dot{x}_{m-1} = x_m \\ \dot{x}_m = \frac{1}{a_n}(-a_1x_1 - a_2x_2 - a_3x_3 - \dots - a_mx_m + b(u + d)) \\ \dot{d} = 0. \end{cases} \tag{12}$$

From (12), an ROPIO can be derived as presented below:

$$\dot{\hat{d}} = l(d - \hat{d}) = \frac{l}{b} (a_n \dot{x}_m + a_1x_1 + a_2x_2 + \dots + a_mx_m - b(u + \hat{d})), \tag{13}$$

where $l > 0$ is the observer gain and \hat{d} is the estimated equivalent disturbance. To avoid the use of the time derivative (\dot{x}_m) in (13), a new variable x_c is defined as

$$x_c = \hat{d} - \frac{l}{b} a_n x_m. \tag{14}$$

Thus, the expression of the ROPIO (13) is rewritten as

$$\begin{cases} \dot{x}_c = -lx_c + \frac{l}{b}(a_1x_1 + a_2x_2 + \dots + (a_m - la_n)x_m) - lu, \\ \hat{d} = x_c + \frac{l}{b} a_n x_m. \end{cases} \tag{15}$$

Subsequently, combining (4) with (15) yields an ROPIO compensated ROMBC given as

$$u = -Kx_{[1,m]} - \hat{d}. \tag{16}$$

The performance of (16) has also been tested on the same DC motor control problem as shown in Figure 3 (with same conditions as the simulation in Figure 2). In the second simulation, the three controllers have been combined with an ROPIO as shown in (16) with an observer gain of $l = 5000$.

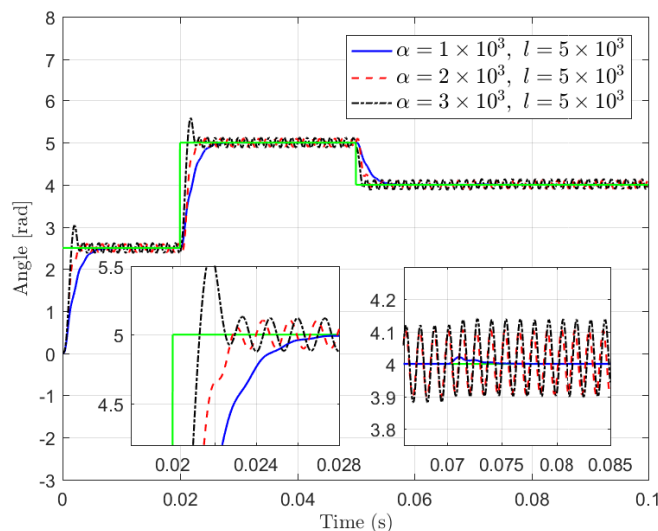


Figure 3. Transient and disturbance rejection performance of ROPIO compensated ROMBC (16).

Contrary to common expectation, combining the ROMBCs with an ROPIO did not improve the unstructured disturbance rejection capacity as shown in Figure 3. The performance of the controllers with $\alpha = 2000$ and $\alpha = 3000$ has degraded as a result of the ROPIO compensation. However, the controller with the lowest value of $\alpha = 1000$ has been improved by the ROPIO (blue line in Figure 3).

It is noted that the ROPIO has not improved the transient state overshoot caused by the relative degree uncertainty (3). To understand the cause behind the ineffectiveness of the ROPIO and eventually propose a solution that can improve the overall performance of the ROMBC, a stability analysis is carried out on the closed-loop system in the following sections.

3.2. Stability Boundary for an ROPIO Compensated ROMBC

When the control law (16) is applied to the original system model (1), the closed-loop system is governed by

$$\begin{cases} \dot{x}_1 = x_2 \\ \dot{x}_2 = x_3 \\ \vdots \\ \dot{x}_m = x_n \\ \dot{x}_n = -a_n \alpha^m x_1 - a_n \binom{m}{m-1} \alpha^{m-1} x_2 - \dots - a_n \binom{m}{2} \alpha^2 x_{m-1} - a_n \left(\binom{m}{1} \alpha + l \right) x_m - a_n x_n - b x_c \\ \dot{x}_c = \frac{l}{b} \left(a_n \alpha^m x_1 + a_n \binom{m}{m-1} \alpha^{m-1} x_2 + \dots + a_n \binom{m}{2} \alpha^2 x_{m-1} + a_n \binom{m}{1} \alpha x_m \right). \end{cases} \quad (17)$$

Since the system matrix is

$$A_{cl} = \begin{bmatrix} 0 & 1 & \dots & 0 & 0 & 0 & 0 \\ 0 & 0 & \dots & 0 & 0 & 0 & 0 \\ \vdots & \vdots & \ddots & \vdots & \vdots & \vdots & \vdots \\ 0 & 0 & \dots & 0 & 0 & 1 & 0 \\ -a_n\alpha^m & -a_n\binom{m}{m-1}\alpha^{m-1} & \dots & -a_n\binom{m}{2}\alpha^2 & -a_n\left(\binom{m}{1}\alpha + l\right) & -a_n & -b \\ \frac{l}{b}a_n\alpha^m & \frac{l}{b}a_n\binom{m}{m-1}\alpha^{m-1} & \dots & \frac{l}{b}a_n\binom{m}{2}\alpha^2 & \frac{l}{b}a_n\binom{m}{1}\alpha & 0 & 0 \end{bmatrix}, \quad (18)$$

one can obtain the characteristic equation of (17) as follows.

$$s^{n+1} + a_n s^n + a_n \left(\binom{m}{1} \alpha + l \right) s^m + \dots + a_n \left(\alpha^m + \binom{m}{m-1} \alpha^{m-1} l \right) s + a_n \alpha^m l = 0. \quad (19)$$

To investigate the relations among α , a_n and l for the stability of (17), (19) is rearranged into the following form for the root locus analysis:

$$1 + \frac{a_n l (s + \alpha)^m}{s(s^n + a_n (s + \alpha)^m)} = 0. \quad (20)$$

Obviously, the root trajectories start from the origin and the roots of (8) on the left-half plane. Out of the $(n + 1)$ root trajectories, m move towards $-\alpha$. As for the remaining two root trajectories, since the centroid σ and asymptotes θ according to l are derived as

$$\sigma = \frac{\alpha m - a_n}{2}, \quad \theta = \pm \frac{\pi}{2}, \quad (21)$$

they move towards $\sigma \pm j\infty$. From (20) and (21), the stability of (17) is satisfied when the gain l is small. In addition, under the condition $\sigma \leq 0$, that is, $\alpha m \leq a_n$, the roots of (19) remain on the left-half plane. To investigate the necessary conditions for l according to α such that (17) is stable, the Routh-Hurwitz criterion is applied. Based on the analysis carried out, a necessary condition is stated as

$$m\alpha \left(a_n - \frac{m-1}{2}\alpha \right) + l(a_n - m\alpha) > 0. \quad (22)$$

The stability condition is summarized by combining (11) and (22), as

$$\begin{cases} 0 < l, & \text{for } 0 < \alpha \leq \frac{a_n}{m}, \\ 0 < l < \frac{m\alpha}{m\alpha - a_n} \left(a_n - \frac{m-1}{2}\alpha \right), & \text{for } \frac{a_n}{m} < \alpha < \frac{2a_n}{m-1}. \end{cases} \quad (23)$$

To further study the boundary of l according to α in (23), the time derivative of $f(\alpha)$, defined below is taken into consideration.

$$f(\alpha) = \frac{m\alpha}{m\alpha - a_n} \left(a_n - \frac{m-1}{2}\alpha \right), \quad (24)$$

$$f'(\alpha) = \frac{df}{d\alpha}(\alpha) = -\frac{m^2(m-1)}{2(m\alpha - a_n)^2} \left(\left(\alpha - \frac{a_n}{m} \right)^2 + \frac{m+1}{m^2(m-1)} a_n^2 \right) < 0. \quad (25)$$

Since $f'(\alpha)$ always has a negative value, it can be concluded that increasing α decreases the range of l for the stability of (17).

For the purpose of validation, the analysis carried out thus far is detailed by applying it to a DC motor position control problem in the next section.

4. Further Analysis Using DC Motor Position Control System

4.1. Boundary Conditions for DC Motor Position Control

Consider a DC motor system described by

$$\begin{cases} \dot{\theta}_m = \omega_m \\ \dot{\omega}_m = -\frac{B_m}{J_m}\omega_m + \frac{K_t}{J_m}i_a \\ \dot{i}_a = -\frac{K_b}{L_a}\omega_m - \frac{R_a}{L_a}i_a + \frac{1}{L_a}u, \end{cases} \quad (26)$$

where θ_m is the rotor angle, ω_m is the velocity, i_a is the armature current, B_m is the friction coefficient, J_m is the rotor inertia, K_b is the back EMF constant, K_t is the torque constant, L_a is the armature inductance, R_a is the armature resistance, and u is the input voltage.

Defining the state vector $x = [x_1 \ x_2 \ x_3]^T = [\theta_m \ \omega_m \ \dot{\omega}_m]^T$, (26) can be put into

$$\begin{cases} \dot{x}_1 = x_2 \\ \dot{x}_2 = x_3 \\ \dot{x}_3 = -a_1x_1 - a_2x_2 - a_3x_3 + bu, \end{cases} \quad (27)$$

where $a_1 = 0$, $a_2 = (B_m R_a + K_b K_t) / (J_m L_a)$, $a_3 = B_m / J_m + R_a / L_a$, and $b = K_t / (J_m L_a)$.

Since the electrical dynamics of practical electric motors is considerably faster than the mechanical ones, (27) can be represented by the reduced-order model

$$\begin{cases} \dot{x}_1 = x_2 \\ \dot{x}_2 = \frac{1}{a_3}(-a_1x_1 - a_2x_2 + b(u + d)), \end{cases} \quad (28)$$

where d represents the equivalent disturbance including the relative degree uncertainty from the model reduction.

Using (4)–(6), the control law that will place all the closed-loop poles at $s = -\alpha$; $\alpha > 0$ is

$$u = -\left(\frac{a_3\alpha^2 - a_1}{b}\right)x_1 - \left(\frac{2a_3\alpha - a_2}{b}\right)x_2. \quad (29)$$

Applying (29) to the original system (27) yields the closed-loop system

$$\begin{cases} \dot{x}_1 = x_2 \\ \dot{x}_2 = x_3 \\ \dot{x}_3 = -a_3\alpha^2x_1 - 2a_3\alpha x_2 - a_3x_3. \end{cases} \quad (30)$$

The characteristic equation of (30) can be rearranged into the following root locus form:

$$1 + \frac{a_3(s + \alpha)^2}{s^3} = 0. \quad (31)$$

Since the departure angles of the root trajectories are $-\pi/3$, $\pi/3$ and π , two roots of (31) move towards the right-half plane as a_3 increases (seen in Figure 1). To find when the root locus crosses the imaginary axis into the left half-plane, applying the Routh-Hurwitz criterion to (31) yields the conditions below.

$$\alpha(2a_3 - \alpha) > 0, \quad a_3\alpha^2 > 0. \quad (32)$$

Since $a_3 > 0$ and $\alpha > 0$, α must satisfy the following condition as in (11):

$$0 < \alpha < 2a_3. \quad (33)$$

By adopting the same approach in Section 3.1, an ROPIO is designed to compensate for the system uncertainties. From (15), the ROPIO is given by

$$\begin{cases} \hat{d} = x_c + \frac{1}{b}a_3x_2, \\ \dot{x}_c = -lx_c + \frac{1}{b}(a_1x_1 + (a_2 - la_3)x_2) - lu. \end{cases} \tag{34}$$

Subsequently, (29) is modified into the following ROPIO compensated ROMBC:

$$u = -\left(\frac{a_3\alpha^2 - a_1}{b}\right)x_1 - \left(\frac{a_3(2\alpha + l) - a_2}{b}\right)x_2 - x_c. \tag{35}$$

Applying (35) to (27) yields the closed-loop system equation

$$\begin{cases} \dot{x}_1 = x_2 \\ \dot{x}_2 = x_3 \\ \dot{x}_3 = -a_3\alpha^2x_1 - a_3(2\alpha + l)x_2 - a_3x_3 - bx_c \\ \dot{x}_c = \frac{1}{b}(a_3\alpha^2x_1 + 2a_3\alpha x_2). \end{cases} \tag{36}$$

Thus, the characteristic equation is given as

$$s^4 + a_3s^3 + a_3(2\alpha + l)s^2 + a_3(\alpha^2 + 2\alpha l)s + a_3\alpha^2l = 0. \tag{37}$$

Before testing the Routh-Hurwitz criterion, (37) is rearranged for the root locus analysis as follows:

$$1 + \frac{a_3l(s + \alpha)^2}{s(s^3 + a_3(s + \alpha)^2)} = 0. \tag{38}$$

Under the condition (33), since the root locus centroid $\sigma = (2\alpha - a_3)/2$ and asymptote $\theta = \pm\pi/2$, the roots are located on the left-half plane when $\sigma \leq 0$, that is, $2\alpha \leq a_3$.

Otherwise, when $2\alpha > a_3$, the system eventually becomes unstable with a large value of l . To find its exact stability boundary, the first column of the Routh-Hurwitz criterion on (37) is derived as

$$s^4 : 1 > 0 \tag{39}$$

$$s^3 : a_3 > 0 \tag{40}$$

$$s^2 : h_{11} = (a_3 - 2\alpha)l + \alpha(2a_3 - \alpha) \tag{41}$$

$$s^1 : h_{21} = \frac{2a_3\alpha(a_3 - 2\alpha)l^2 + 4a_3\alpha^2(a_3 - \alpha)l + a_3\alpha^3(2a_3 - \alpha)}{h_{11}} \tag{42}$$

$$s^0 : h_{31} = a_3\alpha^2l > 0. \tag{43}$$

It can be first observed in (41) that, regardless of the positive gain l , h_{11} is negative when $\alpha > 2a_3$. This implies that the upper boundary of α for the stability of (30) cannot be extended by the ROPIO action. In other words, even though the ROPIO improves system performance against various system uncertainties, it cannot compensate for the effects of the relative degree uncertainty caused by the model order reduction undertaken in the controller design stage.

The necessary and sufficient condition on l in accordance with α for the stability of (36), that is, $h_{11}, h_{21} > 0$, are further investigated as follows. From (41), the boundary condition for $h_{11} > 0$ is readily obtained as

$$\begin{cases} 0 < l & , \text{ for } 0 < \alpha \leq 0.5a_3, \\ 0 < l < \frac{\alpha(2a_3 - \alpha)}{2\alpha - a_3} & , \text{ for } 0.5a_3 < \alpha < 2a_3. \end{cases} \tag{44}$$

Since the denominator of h_{21} is h_{11} , the condition for $h_{21} > 0$ is divided as in (44). In the range $0 < \alpha \leq 0.5a_3$, all the terms in the numerator of h_{21} are positive when $l > 0$.

In the range $0.5a_3 < \alpha < 2a_3$, since the coefficient of the highest order term of the numerator is negative, the quadratic formula is employed to obtain the roots (l_1, l_2) given as

$$l_1 = \frac{\alpha \left(2(a_3 - \alpha) + \sqrt{4(a_3 - \alpha)^2 + 2(2\alpha - a_3)(2a_3 - \alpha)} \right)}{2(2\alpha - a_3)} = \frac{\alpha(2(a_3 - \alpha) + \sqrt{2a_3\alpha})}{2(2\alpha - a_3)}, \quad (45)$$

$$l_2 = \frac{\alpha \left(2(a_3 - \alpha) - \sqrt{4(a_3 - \alpha)^2 + 2(2\alpha - a_3)(2a_3 - \alpha)} \right)}{2(2\alpha - a_3)} = \frac{\alpha(2(a_3 - \alpha) - \sqrt{2a_3\alpha})}{2(2\alpha - a_3)}. \quad (46)$$

Since $l_1 > 0$ and $l_2 < 0$, the condition for $h_{21} > 0$ is

$$\begin{cases} 0 < l, & \text{for } 0 < \alpha \leq 0.5a_3, \\ 0 < l < l_1, & \text{for } 0.5a_3 < \alpha < 2a_3. \end{cases} \quad (47)$$

To identify the intersection of the two boundaries (44) and (47), the difference between the two values is obtained as

$$\frac{\alpha(2a_3 - \alpha)}{2\alpha - a_3} - l_1 = \frac{\alpha\sqrt{2a_3}(\sqrt{2a_3} - \sqrt{\alpha})}{2(2\alpha - a_3)} > 0, \quad \text{for } 0.5a_3 < \alpha < 2a_3. \quad (48)$$

From the above inequality, the boundary condition for the stability of (36) has been proved to be (47). It can be noted that the upper limit l_1 goes to ∞ as $\alpha \rightarrow 0.5a_3$, and a high observer gain will not destabilize the closed-loop system when $0 < \alpha \leq 0.5a_3$ as shown in Figure 4.

At this point, to investigate the impact of α on l_1 in (47), l_1 is realized as

$$l_1 = f(\alpha) = \frac{\alpha(2(a_3 - \alpha) + \sqrt{2a_3\alpha})}{2(2\alpha - a_3)} = \frac{\alpha \left(2 \left(1 - \frac{\alpha}{a_3} \right) + \sqrt{2 \frac{\alpha}{a_3}} \right)}{2 \left(2 \frac{\alpha}{a_3} - 1 \right)}, \quad \text{for } 0.5 < \frac{\alpha}{a_3} < 2. \quad (49)$$

Defining a new variable $\beta^2 := 2\alpha/a_3$, (49) can be rewritten as

$$f(\beta) = \frac{a_3}{4} \cdot \frac{\beta^2(2 - \beta^2 + \beta)}{\beta^2 - 1} = \frac{a_3}{4} \cdot \frac{-\beta^4 + \beta^3 + 2\beta^2}{\beta^2 - 1}, \quad \text{for } 1 < \beta < 2. \quad (50)$$

Taking the derivative of (50) with respect to β yields

$$f'(\beta) = \frac{df(\beta)}{d\beta} = -\frac{a_3}{4} \cdot \frac{\beta(\beta + 1)^2 \left(2\left(\beta - \frac{5}{4}\right)^2 + \frac{7}{8} \right)}{(\beta^2 - 1)^2} < 0, \quad \text{for } 1 < \beta < 2. \quad (51)$$

Thus, the value of l_1 decreases as α increases.

The major implication of (47) is, despite having a separately stable state feedback controller and stable high-gain observer, combining the two does not guarantee a stable closed-loop system if the observer is designed based on a reduced-order model. In other words, there is a trade-off between α and l to maintain the closed-loop system stability. This is further emphasized by (51), which states that as the closed-loop pole value increases, the observer gain must decrease such that the closed-loop system remains stable. Therefore, the separation principle does not hold for the reduced-order model-based ROPIO compensated system. This property can be visualized in Figure 4 for better understanding of the stability boundary conditions.

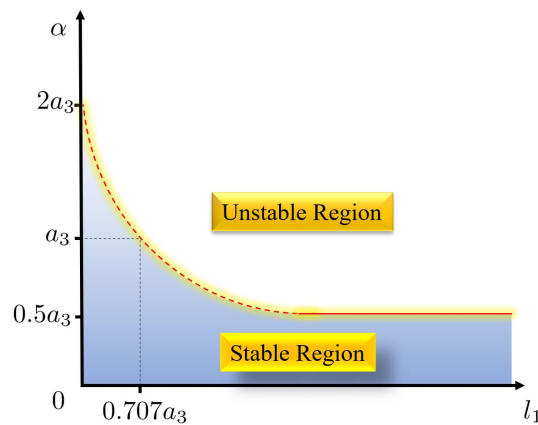


Figure 4. Stability boundary for values of α and l .

4.2. Simulation Studies for Improving Transient and Robust Performance

To validate the theoretical analysis in this paper, computer simulations have been carried out using the system model (26). Based on the parameters in Table 1, one can obtain that $a_3 \approx 2885.8$. At $t = 0.07$ s the magnitude of the step disturbance is 50 V. It should be noted that a control input saturation of 1000 V has been used in the simulations to prevent the controlled output from diverging when the closed-loop system is unstable. This limitation explains why the trajectories in Figure 3 exhibit bounded oscillations while their closed-loop poles are located on the right-half plane as shown in the left root locus plots of Figures 5 and 6.

Table 1. DC Motor System Parameters [12].

Parameter	Value	Unit
R_a	0.605	$[\Omega]$
L_a	0.210	$[\text{mH}]$
K_t	0.0234	$[\text{Nm/A}]$
J_m	86.57	$[\text{g}\cdot\text{cm}^2]$
B_m	4.2167×10^{-2}	$[\text{mNm}/(\text{rad/s})]$
K_b	0.0233	$[\text{V}/(\text{rad/s})]$

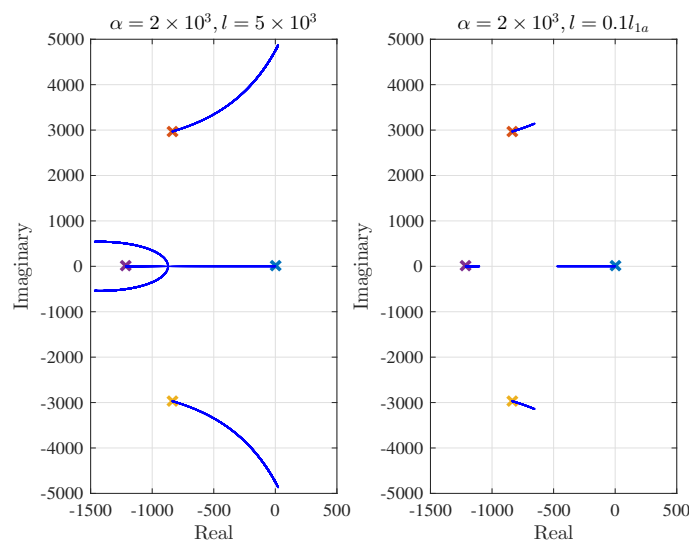


Figure 5. Root trajectories of ROPIO compensated ROMBC when $\alpha = 2000$ for $l = 5000$ (left) and $l = 0.1l_a = 463.95$ (right).

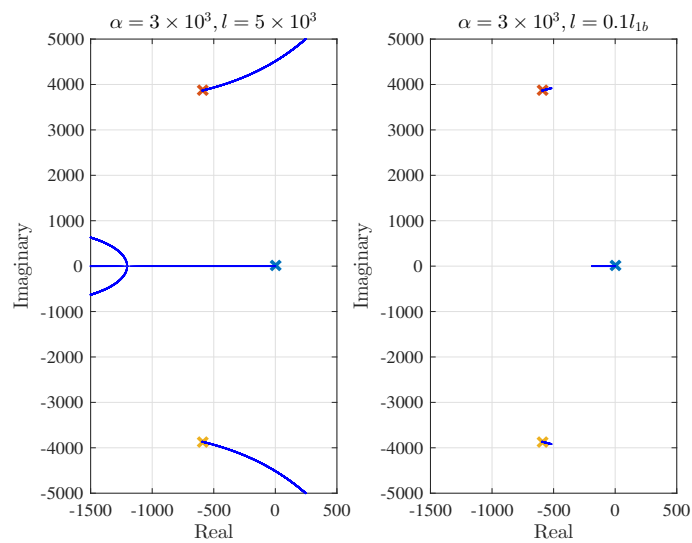


Figure 6. Root trajectories of ROPIO compensated ROMBC when $\alpha = 3000$ for $l = 5000$ (left) and $l = 0.1l_{1b} = 189.43$ (right).

In Figure 7, the simulations of Figure 3 in Section 3.1 are repeated by changing the ROPIO gains in accordance with α , since l_1 decreases as α increases as illustrated in Figure 4. Instead of using $l = 5000$ for all the three controllers in Figure 3, $l = l_a = 0.1l_{1a} = 463.95$ was used for $\alpha = 2000$ and $l = l_b = 0.1l_{1b} = 189.43$ for $\alpha = 3000$. Compared to Figure 3, the disturbance rejection performance (beginning at $t = 0.07$ s) of the controllers with $\alpha = 2000$ and $\alpha = 3000$ has been significantly improved in Figure 7. In particular the controllers with the modified observer gain values: $\alpha = 2000, l = 463.95$ and $\alpha = 3000, l = 189.43$, recovered from the external disturbance within 0.01 s and 0.025 s.

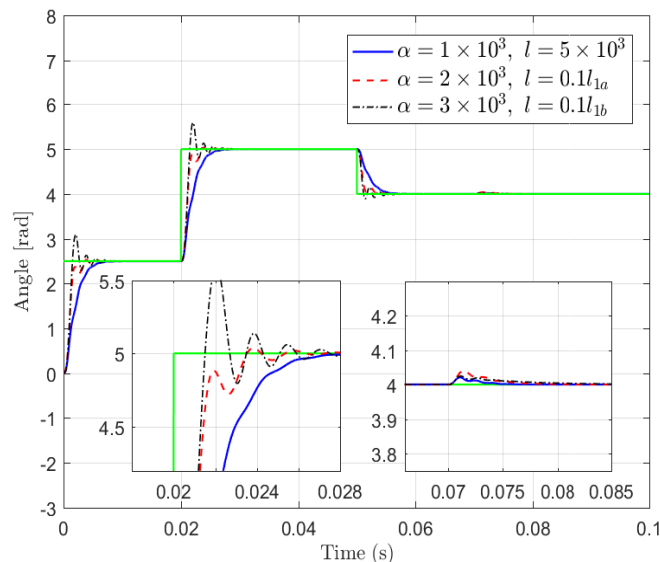


Figure 7. Performance improvement of ROPIO compensated ROMBC with lowered l according to α .

The performance improvement can further be understood by looking at the root locus plots of the two controllers in Figures 5 and 6. Figure 5 exhibits the root locus trajectories of (38) when $\alpha = 2000$ for $0 \leq l \leq 5000$ (left root locus) and $0 \leq l \leq 0.1l_{1a}$ (right one) where $0.1l_{1a} = 463.95$. It can be seen that the left root locus in Figure 5 crosses the imaginary axis into the right half-plane, thus implying that the system becomes unstable by using a large observer gain $l = 5000$. This is owing to the root locus centroid $\sigma > 0$. Because of the input saturation used in the simulation, however, the system response in Figure 3 does not

diverge in the simulation. On the other hand, the right root trajectories in Figure 5 remain in the stable region and the disturbance rejection ability can be improved when the ROPIO gain is adjusted based on the value of α such that it is selected to be under the value of $l_{1a} = 4639.5$ from (49).

A similar conclusion can be reached by observing the root locus plot in Figure 6 when $\alpha = 3000$ and $l_{1b} = 1894.3$ from (49). It is also seen that the starting points of the root locus in Figure 6 have moved rightward when compared to those in Figure 5. Subsequently, the left plot of Figure 6 crosses the imaginary axis faster than that of Figure 5 and the closed-loop system stability deteriorates with $l = 5000$. While using an observer gain less than the value of l_{1b} , for example, $l = 0.1l_{1b}$ allows the disturbance rejection ability of the controller to be improved without altering the stability of the closed-loop system. From the root locus analysis, it is verified that as the closed-loop pole value (α) increases, the observer gain (l) must decrease in order to maintain the closed-loop stability.

Despite the improvement made on the disturbance rejection capability of the controllers, no observable improvement was made on the transient performance in Figure 7. Thereby implying that the ROPIO has no effect on the transient performance of the controller, and the value of α is solely responsible for the transient performance. However, using the information gathered from (47) and the simulations, it can be said that a value of $\alpha < 0.5a_3$ exhibits more stable transient performance compared to higher values of α . Thus, the non-oscillatory transient performance of the controller using $\alpha = 1000$ in Figure 7 is a result of $\alpha = 1000 < 0.5a_3 = 1442.9$. As mentioned in (47), for the range $0 < \alpha < 0.5a_3$, any value of $l > 0$ can be used to improve the controller robustness against external disturbances. This property is further investigated by selecting $\alpha = 0.2a_3$ and studying the overall performance improvement for various values of l in the following simulations.

The purpose of the simulations in Figure 8 is to show that in the first range of α in (47), $0 < \alpha \leq 0.5a_3$, the counted-on characteristics of an observer remain consistent. That is, in this range a higher value of l produces a better disturbance rejection performance. When $\alpha = 0.2a_3$, this property can be noticed in Figure 8 whereby the best performance is obtained from the highest value of the gain $l = 8 \times 10^4$ (black broken line).

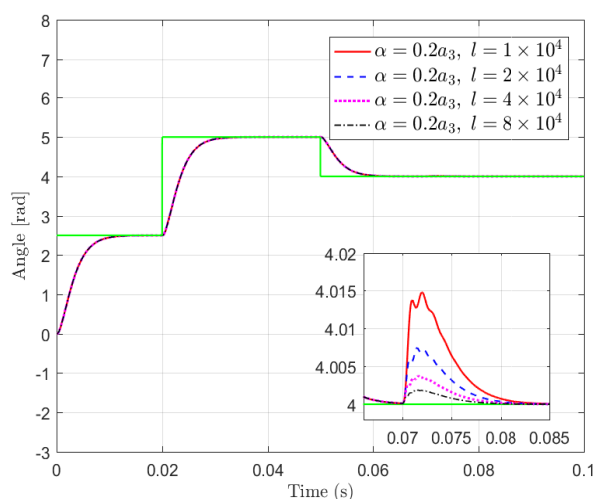


Figure 8. Performance comparison of ROPIO compensated ROMBC by increasing l with $\alpha = 0.2a_3$.

To analyze the performance of the controllers in Figure 8, the root trajectories are presented in Figure 9. As the trajectories approach the infinities of the imaginary axis along a stable asymptote line, a higher observer gain does not risk the closed-loop system stability.

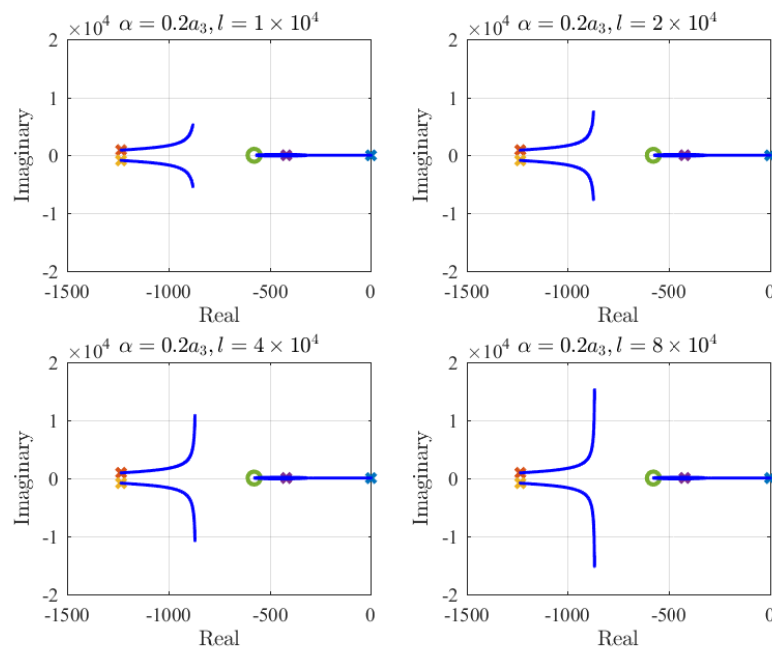


Figure 9. Root trajectories of ROPIO compensated ROMBC by increasing l with $\alpha = 0.2a_3$.

Thus, at this point it is reasonable to pursue a relatively desirable performance that can be attained using the ROPIO compensated ROMBC (35). So far it has been established that the ROMBC can provide a steady transient performance and an adjustable disturbance rejection performance for a value of α in the range $0 < \alpha \leq 0.5a_3$ regardless of the value of l . Therefore, the range $0 < \alpha \leq 0.5a_3$, represented as Region B in Figure 10, is the relatively desirable performance region proposed by this paper. However, the combined region $0 < \alpha \leq 2a_3$ or the union of Region A and Region B in Figure 10 still yields stable response of the ROMBC.

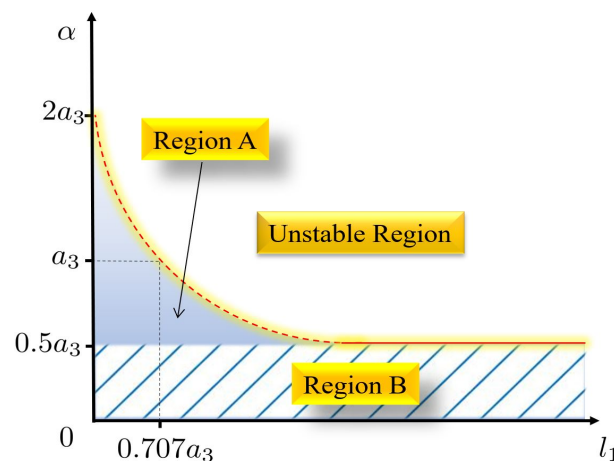


Figure 10. Relatively desirable performance region of ROPIO compensated ROMBC.

The next simulation provides an insight on how the controller performance is affected in Region B as the value of α is increased from $\alpha = 0.2a_3$ to $\alpha = 0.5a_3$. It might be expected that a higher value of α puts the closed-loop poles further away from the imaginary axis and improves the transient performance as α increases. However, Figure 11 shows that at the boundary of Region B, that is when $\alpha = 0.5a_3$, a high observer gain produces a stable but oscillatory performance. While the same value of observer gain does not result this oscillatory response for the controllers with a smaller value of α . This can be further analyzed using their root trajectories.

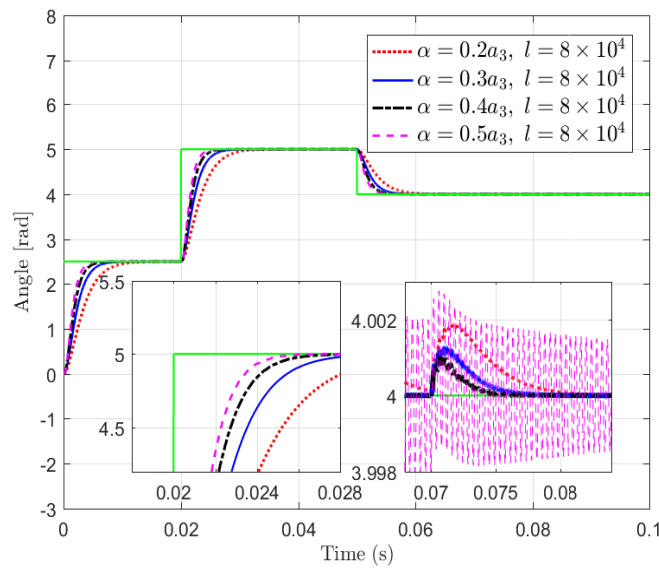


Figure 11. Performance comparison of ROPIO compensated ROMBC by increasing α with $l = 8 \times 10^4$.

In the root locus plots in Figure 12, it is seen that as the value of α increases the root trajectories approach the imaginary axis. Thus, the most crucial information gathered from this revelation is the existence of a trade-off between transient performance and disturbance rejection ability for the ROPIO compensated ROMBC. Increasing the value of α improves transient performance, while reducing its flexibility to work with high-gain observer that can be used to improve robustness against system uncertainties and external disturbances.

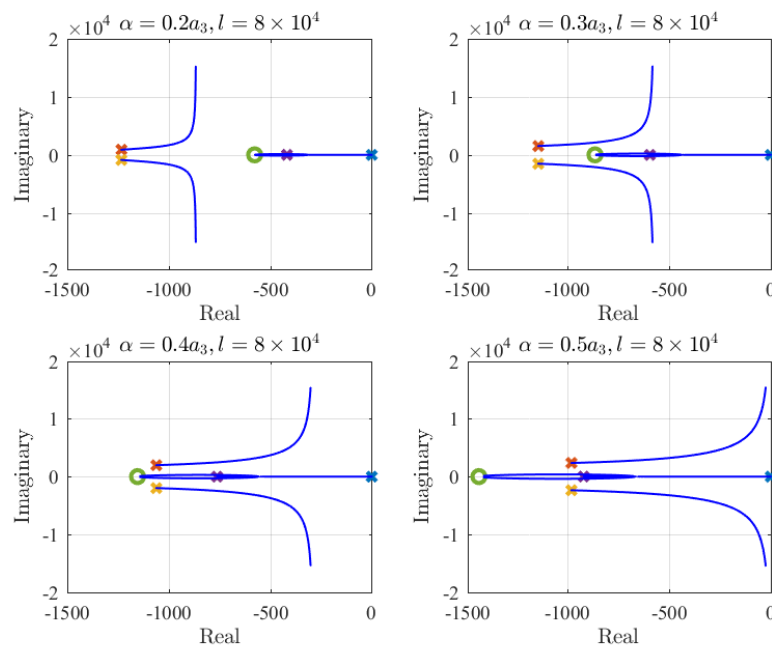


Figure 12. Root trajectories of ROPIO compensated ROMBC by increasing α with $l = 8 \times 10^4$.

From the simulations carried out so far, it is concluded that the desirable performance obtained from the ROMBC is by using a value of α near $0.4a_3$ (black broken line plot in Figure 11). At this value of α , the state feedback controller produces a satisfactory transient performance while not risking instability caused by high-gain observers.

5. Conclusions

Since the effects of the ignored fast dynamics are reflected by poor transient and robust performance, this paper provides the stability analysis of a reduced-order model-based state feedback controller (ROMBC) combined with a reduced-order proportional-integral observer (ROPIO) via the root locus approach and the Routh-Hurwitz stability criterion. The stability boundary condition from the theoretical analysis reveals that, in order for the closed-loop system stability to be maintained, the value of the observer gain must decrease as the feedback controller pole increases. This implies that there exists a break from the separation principle for a reduced-order model-based observer and state feedback controller.

A variety of computer simulations have been performed on a DC motor position control problem to examine the transient performance and the disturbance rejection ability of the ROPIO compensated ROMBC. Contrary to common expectations rather than improving the control system's overall performance, the mathematical analysis and the simulations have shown that there exists a trade-off between transient state performance and disturbance rejection ability. The paper concluded by recommending a region based on the closed-loop pole and observer gain value that provided a relatively preferable performance for an ROPIO compensated ROMBC. Future studies could fruitfully explore the effects of employing a different type of controller methods such as a Linear Quadratic Regulator (LQR) with a disturbance observer to improve robustness of an ROMBC with a larger model order reduction.

Author Contributions: Conceptualization, Y.I.S.; simulation works, experiments, and theoretical analysis, N.D.A., D.H.K., S.J.Y., and Y.I.S.; writing—original draft preparation, N.D.A., D.H.K., and Y.I.S.; and writing—review and editing, N.D.A., S.J.Y., and Y.I.S.; supervision, Y.I.S. All authors have read and agreed to the published version of the manuscript.

Funding: This research was supported by Korea Electric Power Corporation. (Grant number: R17XA05-2) This work was supported by the National Research Foundation of Korea(NRF) grant funded by the Korea government(MSIT) (No. 2019R1F1A1058543).

Institutional Review Board Statement: Not applicable.

Informed Consent Statement: Not applicable.

Conflicts of Interest: The authors declare no conflict of interest.

Abbreviations

The following abbreviations are used in this manuscript:

ROMBC	Reduced-Order Model-Based Controller
ROPIO	Reduced-Order Proportional-Integral Observer

References

1. Franklin, G.F.; Powell, J.D.; Emami-Naeini, A. *Feedback Control of Dynamic Systems*, 5th ed.; Prentice-Hall: Upper Saddle River, NJ, USA, 2005; pp. 20–454.
2. Kokotović, P.; Khalil, H.K.; O'Reilly, J. *Singular Perturbation Methods in Control: Analysis and Design*; SIAM: Philadelphia, PA, USA, 1999; pp. 1–43.
3. Skogestad, S.; Postlethwaite, I. *Multivariable Feedback Control: Analysis and Design*; John Wiley & Sons, Inc.: New York, NY, USA, 2005; pp. 479–498.
4. Khalil, H.K. *Nonlinear Systems*, 3rd ed.; Prentice-Hall: Upper Saddle River, NJ, USA, 2002; pp. 432–460.
5. Li, C.; Du, Z.; Ni, Y.; Zhang, G. Reduced model-based coordinated design of decentralized power system controllers. *IEEE Trans. Power Syst.* **2016**, *31*, 2172–2181. [[CrossRef](#)]
6. Yao, J.; Jiao, Z.; Ma, D. Adaptive robust control of DC motors with extended state observer. *IEEE Trans. Ind. Electron.* **2014**, *61*, 3630–3637. [[CrossRef](#)]
7. Yook, J.H.; Kim, I.H.; Son, Y.I. Robustness improvement of DC motor speed control using communication disturbance observer under uncertain time delay. *Electron. Lett.* **2017**, *53*, 389–391. [[CrossRef](#)]
8. Saha, S.; Amrr, S.M.; Nabi, M.U.; Iqbal, A.A. Reduced-order modeling and sliding mode control of active magnetic bearing. *IEEE Access* **2019**, *7*, 113324–113334. [[CrossRef](#)]

9. Anandan, P.; Gagliano, S.; Bucolo, M. Computational models in microfluidic bubble logic. *Microfluid. Nanofluid.* **2015**, *18*, 305–321. [[CrossRef](#)]
10. Li, S.; Yang, J.; Chen, W.H.; Chen, X. *Disturbance Observer-Based Control: Methods and Applications*; CRC Press: Boca Raton, FL, USA, 2014.
11. Shim, H.; Jo, N.H. An almost necessary and sufficient condition for robust stability of closed-loop systems with disturbance observer. *Automatica* **2009**, *45*, 296–299. [[CrossRef](#)]
12. Son, Y.I.; Kim, I.H.; Choi, D.S.; Shim, H. Robust cascade control of electric motor drives using dual reduced-order PI observer. *IEEE Trans. Ind. Electron.* **2015**, *62*, 3672–3682. [[CrossRef](#)]
13. Chen, W.H.; Yang, J.; Guo, L.; Li, S. Disturbance-observer-based control and related methods-an overview. *IEEE Trans. Ind. Electron.* **2016**, *63*, 1083–1095. [[CrossRef](#)]
14. Kim, I.H.; Son, Y.I. Regulation of a DC/DC boost converter under parametric uncertainty and input voltage variation using nested reduced-order PI observers. *IEEE Trans. Ind. Electron.* **2017**, *64*, 552–562. [[CrossRef](#)]
15. Sariyildiz, E.; Oboe, R.; Ohnishi, K. Disturbance observer-based control and its application: 35th anniversary overview. *IEEE Trans. Ind. Electron.* **2020**, *67*, 2042–2053. [[CrossRef](#)]
16. Kim, I.H.; Son, Y.I. Design of a low-order harmonic disturbance observer with applications to a DC motor position control. *Energies* **2020**, *13*, 1020. [[CrossRef](#)]
17. Amare, N.D.; Son, Y.I.; Lim, S. Dual PIO-based controller design for robustness improvement of a magnetic levitation system. *J. Electr. Eng. Technol.* **2020**, *15*, 1389–1398. [[CrossRef](#)]
18. Wu, M.; Gao, F.; Yu, P.; She, J.; Cao, W. Improve disturbance-rejection performance for an equivalent-input-disturbance-based control system by incorporating a proportional-integral observer. *IEEE Trans. Ind. Electron.* **2020**, *67*, 1254–1260. [[CrossRef](#)]
19. Jo, N.H.; Joo, Y.J.; Shim, H. A study of disturbance observers with unknown relative degree of the plant. *Automatica* **2014**, *50*, 1730–1734. [[CrossRef](#)]